ChemComm

COMMUNICATION

View Article Online
View Journal | View Issue

Cite this: *Chem. Commun.*, 2020, **56**, 13373

Received 9th September 2020,
Accepted 1st October 2020

DOI: 10.1039/d0cc06101h

rsc.li/chemcomm

Nanoscale crystal grain characterization *via* linear polarization X-ray ptychography†

Zirui Gao, [ab] Mirko Holler, [a] Michal Odstrcil, [a] Andreas Menzel, [a] Manuel Guizar-Sicairos *[a] and Johannes Ihli *[a]

X-ray linear dichroism and X-ray birefringence microscopy are yet to be fully utilized as instruments in the microstructural characterization of crystalline materials. Here, we demonstrate analyser-free X-ray linear dichroism microscopy using spectroscopic hard X-ray ptychography. First experiments enabled a spectroscopic and microstructural characterisation of polycrystalline vanadium pentoxide on the nanoscale, outside of diffraction-contrast based methods.

X-ray linear dichroism-[1–5] and X-ray birefringence microscopy[6–8] measure local changes of a material's refractive index as a function of incident beam polarization and energy. These measurements are commonly conducted in the vicinity of or across an X-ray absorption edge or resonant energy, associated with a chemical element of the material.[8] Probing the spectral response of this element at multiple polarization states of the illumination allows the extraction of local orientational properties, *e.g.* bond anisotropies.[2,8] This is possible as near-edge spectra, frequently the pre-peak region, are sensitive to the coordination geometry of the chemical element relative to the electric field vector of the illumination.[1] Or in other words the sample-relative linear polarisation state of the illumination.

This polarization dependency, similar to the optical polarization microscope,[10] allows in the case of materials with a net-orientation or anisotropy, *e.g.* most non-cubic and some cubic crystalline materials, the characterisation of crystal grains (CGs) within polycrystalline, composite or hierarchically structured materials.[2,4,6,7] Characterisation here refers to shape and size determination of grains, as well as unique orientation determination[2,7] when extended to vector tomography.[11] Yet, such microstructural characterisation is hardly ever performed using X-ray microscopy modalities based on a linear polarization imaging contrast (PIC). Such limited use compared to diffraction-contrast-based methods is largely a result of three factors. One being the commonly weak signal emergent from linear polarization mechanisms, leading to strict signal-to-noise ratio requirements for measurements. Two, existing high-resolution implementations require intricate sample preparation, *e.g.* approaches based on photoemission electron microscopy operate at low X-ray energies and require thin, flat, and surface conductive samples.[2–4] Three, other implementations require either a polarizer-analyser setup or extensive prior knowledge of the specimen.[6,12]

Here, we demonstrate the utilisation of a linear polarization imaging contrast in an analyser-free spectroscopic X-ray ptychography framework and show how it can lessen the restraints posed by existing PIC microscopy methods. X-ray ptychography is an imaging technique that combines scanning transmission X-ray microscopy with lensless computational imaging.[13,14] Ptychography allows the retrieval of the complex-valued transmission function of the imaged sample, *i.e.* images of both absorption and phase contrast are obtained. The spatial resolution of these images is in theory limited only by the detectable angular extent of the specimen-scattered intensity.[13,14] Currently attainable are images below 10 nm spatial resolution[15] with an apparently improved signal-to-noise ratio compared to conventional X-ray microscopy methods.

In these first experiments we characterized the spectral response of vanadium pentoxide (α-V_2O_5) grains to mutually orthogonal polarization states, $\varphi = 0^\circ$ and $\varphi = 90^\circ$. Two ptychographic image series, one per polarization state, were acquired across the vanadium K-edge, 5460–5520 eV, with a maximum step size of 1 eV. Fig. 1a displays the corresponding analyser-free "PIC-Ptychography" acquisition scheme. Using Fourier ring correlation, the full-period spatial-resolution of individual ptychographic image reconstructions was estimated to be 110.4 nm for the phase component and 183 nm for the absorption component. The spatial resolution of the complex-valued image is 119.2 nm. For further details, regarding acquisition, image reconstruction and resolution evaluation please

[a] *Paul Scherrer Institut, 5232 Villigen PSI, Switzerland. E-mail: manuel.guizar-sicairos@psi.ch, johannes.Ihli@psi.ch*
[b] *ETH Zurich, Department of Information Technology and Electrical Engineering, 8093 Zurich, Switzerland*

† Electronic supplementary information (ESI) available: Materials and methods, resolution evaluation, corroborating electron and optical micrographs. See DOI: 10.1039/d0cc06101h

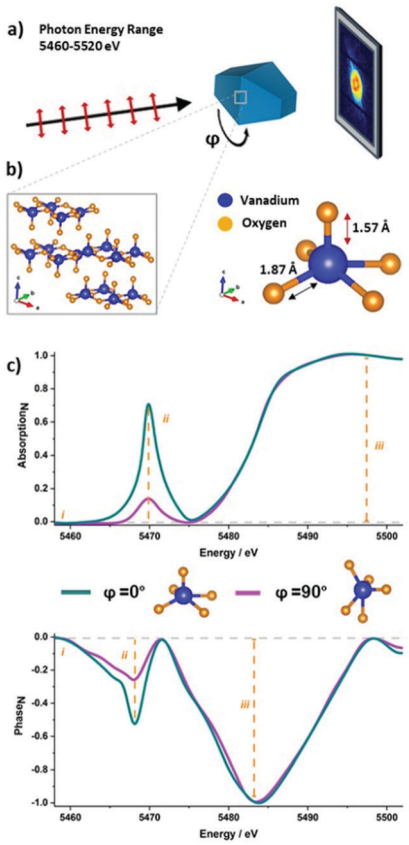

Fig. 1 Linear polarization dependent X-ray ptychography of a vanadium pentoxide crystal. (a) Schematic representation of PIC-ptychography data acquisition. Using monochromatic, coherent X-rays of fixed linear polarisation, two hyperspectral ptychographic image series were acquired across the V K-edge (5460 to 5520 eV). Following the acquisition of the first series the sample holder was azimuthally rotated from, φ = 0 (-) to φ = 90° (-) around the axis of beam propagation, to create the required relative change in incident polarisation state. Shown in turquoise is a 3D Wulff construction of a vanadium pentoxide (V_2O_5) single crystal with the provided coordinate system denoting the main crystallographic axis. (b) Graphical depiction of V_2O_5 layered orthorhombic crystal structure (□), composed of distorted [VO_5] square pyramids. To note is the shorter apical bond (|) of these pyramids, aligned parallel to the crystallographic *c*-axis of the crystal (↑), causing an anisotropic electron density distribution and giving rise to the here utilized X-ray linear dichroism.[9] (c) Example vanadium K-edge spectra collected of an apparent single crystal at 0 and 90° sample rotation, stressing the intensity variation in the pre-edge as well as the location of study-relevant features (–). Features include (i) the projected refractive index retrieved from measurements below the vanadium K-edge. (ii) Pre-peak intensity variations reflective of the apical bond orientation at (5468 & 5070 eV). (iii) Edge jump magnitude in absorption and negative peak height in phase to extract local vanadium concentrations.

see the Methods as well as Fig. S1 and S2 (ESI†). For an animation of the spectral image series at both polarisation states, please see Movie 1 (ESI†).

Vanadium pentoxide was selected for these initial experiments due to its potential use as cathode material[16,17] and heterogeneous catalyst.[18] For both applications, functionality is dependent on grain size, crystallinity, orientation, and morphology of the material. Moreover, the intensity of the pre-peak is known to be sensitive towards the relative incident beam polarisation.[19] This sensitivity, as described in Horrocks *et al.* (2016), is a result of the layered crystal structure of vanadium pentoxide.[19] Vanadium pentoxide is composed of alternating and distorted [VO_5] square pyramids. By distorted we refer to the fact that each pyramid possesses a shorter apical V–O bond compared to the bonds that make up the base of the pyramid.[19] Such a vanadium coordination geometry results in a stronger oxide – X-ray interaction, or pre-peak intensity, when the electric field vector of the illumination is more aligned with the apical bond of the pyramids. See Fig. 1b for a graphical representation.

Fig. 1c shows the absorption and phase spectra of a V_2O_5 crystal at orthogonal polarization states. These spectra demonstrate the pre-peak sensitivity towards changes in polarisation, a sensitivity that is visible in both the absorption and the phase spectra. Further, highlighted in Fig. 1c are study-relevant material properties that can be extracted from either of these spectra. The former being (i) the projected refractive index retrieved from image reconstructions acquired below the vanadium K-edge, here at 5460 eV. (ii) The local vanadium coordination geometry or apical bond orientation extracted from pre-peak intensity variations. In the phase spectra, the pre-peak centre is located at 5468 eV. In the absorption spectra, we find the centre at 5470 eV. (iii) Local projected vanadium concentrations retrieved from either the edge jump magnitude in absorption or negative peak height in phase after baseline correction.

Provided in Fig. 2 are property corresponding distribution maps of two polycrystalline V_2O_5 particles, at orthogonal linear polarization states. Due to the single-component nature of the sample, (i) projected refractive index and (iii) vanadium-concentration maps are proportional to each other, *i.e.* both are reflective of local integrated thickness variations, and thusly appear similar to each other. Furthermore, based on the measured changes in the complex-valued transmission function and the known sample composition, these properties were converted to (i) local thickness and (iii) projected vanadium concentrations. This is shown in Fig. 2a on the example of phase-based image reconstructions. Moreover, it is evident in Fig. 2a that the extracted thickness and concentration maps are hardly affected, as expected, by a relative polarisation change of the incident illumination.

Fig. 2b shows pre-peak intensity maps of both phase and absorption contrast after normalization by the integrated vanadium concentration. These maps show a substantial change in the pre-peak intensity distribution as the sample-relative polarisation state of the illumination is changed from φ = 0° to 90°. Given the polycrystalline nature of the sample, this polarisation sensitivity is even visible in a single polarisation-state map, in which we already see the emergence of spatial domains of near-equal pre-peak intensity. Considering the vanadium-concentration normalization, the existence of these domains can be related to a common orientation of the apical bond and as such to the crystallographic *c*-axis of a particular or a set of V_2O_5 grains. A comparison of local pre-peak intensities across the mutually orthogonal polarization states confirms than that the observed differences indeed arise from CGs of different orientation. Note the expected gain or reduction in pre-peak

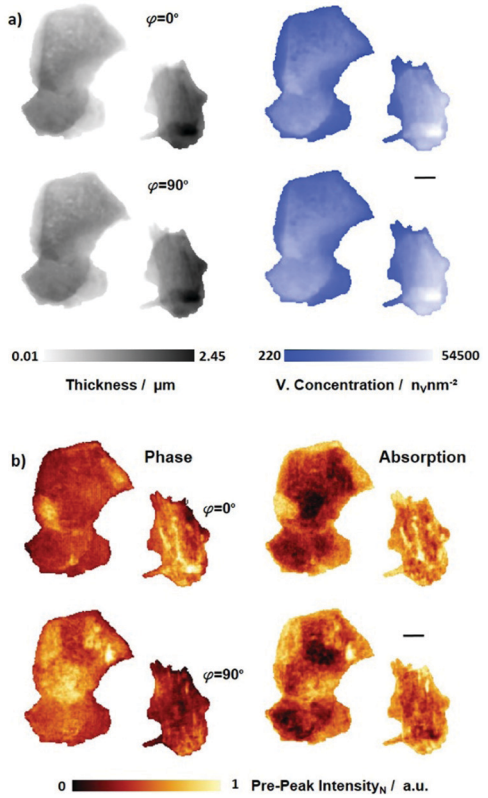

Fig. 2 Ptychographic image reconstructions of polycrystalline V_2O_5 particles at mutually orthogonal polarizations. (a) Thickness and vanadium concentration maps of two polycrystalline V_2O_5 particles at orthogonal linear polarization states (φ = 0° and φ = 90°). Maps were extracted from the phase component of ptychographic vanadium K-edge image series. The thickness map follows a colour map running from white to black, with black indicating the thickest part of the sample, the vanadium concentration colour map runs from blue to white, with white areas indicating areas of highest vanadium concentration. (b) Pre-peak intensity maps at φ = 0° (top) to φ = 90° (bottom) extracted from the same image series. Shown are the phase (left) and the absorption (right) pre-peak intensity response to changes in linear polarisation. Pre-peak intensities are normalized to the vanadium concentration. Pixel size is 48.8 nm. Scale bars are 1 µm.

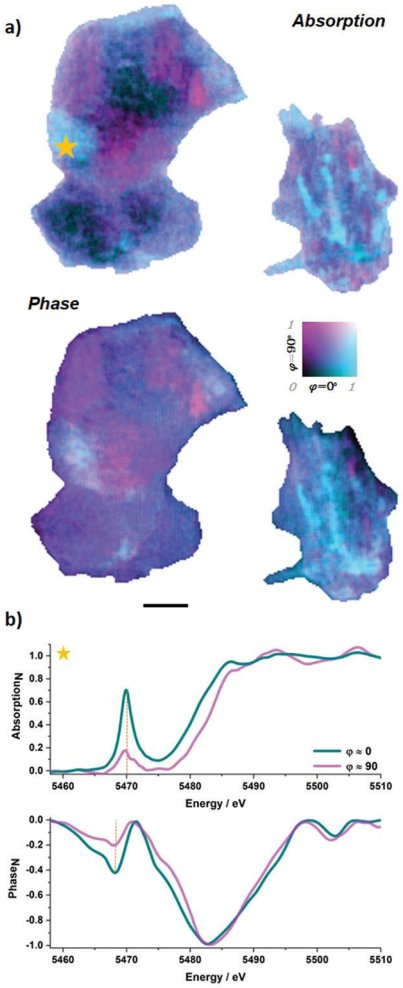

Fig. 3 Grain map and local spectral response of polycrystalline vanadium pentoxide particles. (a) Absorption and phase based grain maps. Maps were constructed by merging V K-edge pre-peak intensity image reconstructions acquired at orthogonal polarization states. A bivariate colour map is used to highlight the alignment of the different V_2O_5 grains, *i.e.* the orientation of the apical bond of the [VO_5] unit, with the incident polarisations. Note that quantitative angular orientations of the crystallographic *c*-axis cannot be obtained with only two polarizations. Scale bar is 1 µm. (b) Pixel-level X-ray near-edge absorption and phase spectra acquired from a polycrystalline vanadium pentoxide particle at mutually orthogonal polarization states. A star in (a) highlights the location of the pixel. Spectra are post-edge normalized and smoothed by 3-point adjacent-averaging.

intensity in selected domains when the linear polarisation is changed. Other domains, conversely, only show minimal intensity variation, this is expected for several scenarios: one, the case where the orientation of the crystallographic *c*-axis is perpendicular to the imaging plane or at 45 degrees to both tested polarisation states, two, the potential presence of amorphous domains, and three, if multiple randomly oriented grains are in the path of the X-ray beam. Due to their random orientation and number, such an ensemble average will exhibit a lower intensity variation when the sample-relative linear polarisation state is changed. For example, the pre-peak intensity loss of one grain might fully or partially be offset by the intensity gain of another or multiple equally illuminated grain(s) of a different orientation. Importantly, these pre-peak intensity maps are not only in morphological agreement with scanning electron micrographs (SEM), Fig. S3 (ESI†), but also partially match the visible grains therein. The partial match in grain identification is due to the SEM being surface-sensitive and thereby only probing the outermost or surface-running grains, while PIC-Ptychography is acquired in transmission geometry and as such probes the entire sample thickness, *i.e.* surface-buried grain boundaries are only visible in the latter.

As shown in Fig. 3a, the acquired pre-peak intensity maps of both polarisations can be combined to obtain a map of the dominant CGs in the two-polycrystalline particles. It should be noted that with two polarizations quantitative orientation maps of the *c*-axis cannot be obtained. In the smaller V_2O_5 particle several surface-running grains are visible in both phase and absorption contrast. These grains, roughly 200 nm in diameter, share a common orientation among each other and are most

likely a result of a secondary nucleation process. The larger particle consists of multiple nearly micron-sized domains. While pairs of these domains appear to share a common orientation, indicative of a preferred crystallographic orientation, the variation in orientation between these pairs appears moderately large, which suggests this arrangement to have originated from particle aggregation during the synthesis or the annealing process. This grain map is corroborated so far possible by micrographs acquired with an optical polarizing microscope, which are shown in Fig. S4 (ESI†).

In contrast to the measured difference in spatial resolution, grain maps extracted from the phase, shown in Fig. 3a, do not appear to be significantly improved compared to the absorption. The basis behind this observation can be seen in Fig. 3b, which shows pixel-level spectra at orthogonal polarisation states. Evident in these spectra is that the difference between the maximum pre-peak intensity in the absorption spectra across polarisations is nearly twice that of the phase. This suggests the phase is less sensitive to changes in polarization, similar to the observation made within the context of X-ray magnetic circular dichroism (XMCD).[11] A second explanation emerges from a closer look at the phase spectra. The pre-peak in the phase spectra possesses a larger spread in energy. This spread of the signal among different energies reduces the maximum contrast in the current and previous means of evaluation. Such spread may in the future encourage fitting of the pre-peak to attain a better result or possibly allow the extraction of secondary information from the phase pre-peak, *e.g.* a more detailed view into the probed coordination geometry.

In summary, we have introduced a technique for linear-polarization-dependent nano-imaging. The method uses X-ray linear dichroism ptychographic-spectroscopy and is analyser-free. The current demonstration with two polarization states provides contrast between grains at different crystalline orientations, but with two polarizations is limited to qualitative grain orientation maps. Quantitative characterisation and associated unique mapping of *c*-axis orientations,[2] becomes possible with additional relative orientations of the sample, and possibly the incorporation of a vectorial ptychography formalism.[10,20,21] The presented 2D approach will find application, for example, within an *in situ* characterisation context of intercalation materials or energy storage materials.[22,23] However, to fully exploit the penetration depth of hard X-rays, future efforts are placed in the combination of PIC-ptychography and computed tomography, specifically vector tomography.[11,24] The associated acquisition of additional tomographic orientations of the sample allows a sensitivity to the out-of-plane component in 3D. This combination would open a new investigative space, in particular for ptychographic X-ray computed tomography (PXCT) studies for which large parts of the scientific interest not only stem from composition and structural variation of the sample, as commonly retrieved in PXCT measurements, but also, and additionally, from grain characteristics and their orientational distribution. Such capabilities would find ubiquitous applications in biomineral,[4] energy storage,[25,26] heterogeneous catalysis,[27] and additive manufacturing research.[28]

The raw data can be obtained under DOI: 10.5281/zenodo.4059817.

We acknowledge the support of the Swiss National Science Foundation (PZ00P2_179886 and 200021_178788).

Conflicts of interest

There are no conflicts to declare.

Notes and references

1 H. Ade and B. Hsiao, *Science*, 1993, **262**, 1427–1429.
2 P. U. P. A. Gilbert, *Microsc. Microanal.*, 2018, **24**, 454–457.
3 R. T. DeVol, C.-Y. Sun, M. A. Marcus, S. N. Coppersmith, S. C. B. Myneni and P. U. P. A. Gilbert, *J. Am. Chem. Soc.*, 2015, **137**, 13325–13333.
4 C. A. Stifler, N. K. Wittig, M. Sassi, C.-Y. Sun, M. A. Marcus, H. Birkedal, E. Beniash, K. M. Rosso and P. U. P. A. Gilbert, *J. Am. Chem. Soc.*, 2018, **140**, 11698–11704.
5 K. Sato, K. Okitsu, Y. Ueji, T. Matsushita and Y. Amemiya, *J. Synchrotron Radiat.*, 2000, **7**, 368–373.
6 B. A. Palmer, S. P. Collins, J. Hulliger, C. E. Hughes and K. D. M. Harris, *J. Am. Chem. Soc.*, 2016, **138**, 16188–16191.
7 B. A. Palmer, G. R. Edwards-Gau, B. M. Kariuki, K. D. M. Harris, I. P. Dolbnya and S. P. Collins, *Science*, 2014, **344**, 1013–1016.
8 Y. Zhou, R. Patterson, B. A. Palmer, G. R. Edwards-Gau, B. M. Kariuki, N. S. S. Kumar, D. W. Bruce, I. P. Dolbnya, S. P. Collins, A. Malandain and K. D. M. Harris, *Chem. Sci.*, 2019, **10**, 3005–3011.
9 K. Momma and F. Izumi, *J. Appl. Crystallogr.*, 2011, **44**, 1272–1276.
10 M. Odstrčil, *Doctoral thesis*, Chapter 2 and 3, University of Southampton, 2017.
11 C. Donnelly, M. Guizar-Sicairos, V. Scagnoli, S. Gliga, M. Holler, J. Raabe and L. J. Heyderman, *Nature*, 2017, **547**, 328.
12 H. Chang, M. A. Marcus and S. Marchesini, arXiv, 2020, arXiv: 2002.04161 [physics.optics].
13 P. Thibault, M. Dierolf, A. Menzel, O. Bunk, C. David and F. Pfeiffer, *Science*, 2008, **321**, 379–382.
14 F. Pfeiffer, *Nat. Photonics*, 2018, **12**, 9–17.
15 J. Vila-Comamala, A. Diaz, M. Guizar-Sicairos, A. Mantion, C. M. Kewish, A. Menzel, O. Bunk and C. David, *Opt. Express*, 2011, **19**, 21333–21344.
16 S. Wang, Z. Lu, D. Wang, C. Li, C. Chen and Y. Yin, *J. Mater. Chem.*, 2011, **21**, 6365–6369.
17 J. Liu, H. Xia, D. Xue and L. Lu, *J. Am. Chem. Soc.*, 2009, **131**, 12086–12087.
18 I. E. Wachs, *Dalton Trans.*, 2013, **42**, 11762–11769.
19 G. A. Horrocks, E. J. Braham, Y. Liang, L. R. De Jesus, J. Jude, J. M. Velázquez, D. Prendergast and S. Banerjee, *J. Phys. Chem. C*, 2016, **120**, 23922–23932.
20 P. Ferrand, A. Baroni, M. Allain and V. Chamard, *Opt. Lett.*, 2018, **43**, 763–766.
21 X. Zhang, B. Cheng, C. Liu, W. Shen and J. Zhu, *Opt. Express*, 2017, **25**, 30851–30861.
22 A. Van der Ven, J. Bhattacharya and A. A. Belak, *Acc. Chem. Res.*, 2013, **46**, 1216–1225.
23 C. Wei, Y. Hong, Y. Tian, X. Yu, Y. Liu and P. Pianetta, *J. Synchrotron Radiat.*, 2020, **27**, 713–719.
24 J. Ihli, R. R. Jacob, M. Holler, M. Guizar-Sicairos, A. Diaz, J. C. da Silva, D. Ferreira Sanchez, F. Krumeich, D. Grolimund, M. Taddei, W. C. Cheng, Y. Shu, A. Menzel and J. A. van Bokhoven, *Nat. Commun.*, 2017, **8**, 809.
25 E. H. R. Tsai, J. Billaud, D. F. Sanchez, J. Ihli, M. Odstrčil, M. Holler, D. Grolimund, C. Villevieille and M. Guizar-Sicairos, *iScience*, 2019, **11**, 356–365.
26 F. Zheng, M. Kotobuki, S. Song, M. O. Lai and L. Lu, *J. Power Sources*, 2018, **389**, 198–213.
27 N. Mizuno and M. Misono, *Chem. Rev.*, 1998, **98**, 199–218.
28 W. E. Frazier, *J. Mater. Eng. Perform.*, 2014, **23**, 1917–1928.

